Russian Chemical Reviews **73** (9) 847 – 860 (2004) © 2004 Russian Academy of Sciences and Turpion Ltd

DOI 10.1070/RC2004v073n09ABEH000917

Complex manganese oxides with the brownmillerite structure: synthesis, crystal chemistry and properties

A M Abakumov, M G Rozova, E V Antipov

Contents

I.	Introduction	847
II.	General information on the crystal structure of brownmillerites $A_2BB'O_5$	848
III.	Synthesis of Mn-containing brownmillerites	851
IV.	The crystal structure of $A_2MnB'O_{5+\delta}$ (A = Ca, Sr; B′ = Ga, Al; $\delta \approx 0$)	851
V.	Specific pattern of the oxidation of brownmillerites $A_2MnGaO_{5+\delta}$ (A = Ca, Sr)	854
VI.	Complex oxofluorides $Sr_2MnGaO_{5-x}F_{1+x}$	856
VII.	Magnetic and transport properties of brownmillerites $A_2MnB'O_{5+\delta}$ (A = Ca, Sr; B′ = Ga, Al) and their derivatives	857
VIII.	The oxide $Ca_{2.5}Sr_{0.5}GaMn_2O_8$ as the second member of the homologous series of brownmillerite-like structures	858
IX.	Conclusion	858

Abstract. Structural features and methods for the synthesis of complex manganese oxides with the brownmillerite structure $A_2MnB'O_{5+\delta}$ (A = Ca, Sr; B′ = Ga, Al) and of their derivatives are surveyed. Modern approaches to the description of crystal structures containing various types of chains of tetrahedra are considered and possible ordering patterns of these chains are discussed. The effects of the electronic structure and crystal chemical properties of the B′ cations on the possibility of formation of a layered ordered structure is noted. The emphasis is placed on the anion non-stoichiometry of the brownmillerite phases and the influence of the excess oxygen (fluorine) on the structure of the compounds. A comparative analysis of properties of oxygen- and fluorine-doped brownmillerites is given. The data on the magnetic structures, transport and magnetoresistive properties of Mn-containing brownmillerites are generalised. The bibliography includes 74 references.

I. Introduction

Among complex manganese oxides, oxides with a general stoichiometry $Ln_{1-x}A_xMnO_3$ (where Ln is a rare-earth cation and A = Ca, Sr, Ba) are most thoroughly studied primarily due to the fact that many representatives of this class manifest colossal magnetoresistance† (see Refs 1 – 6). These compounds possess perovskite-like structures (Fig. 1 *a*) and are characterised by complex correlations between their compositions, crystal structures and physical properties. The magnetic and electronic properties of manganites are usually interpreted within the double exchange theory, which considers the electron transfer between adjacent Mn^{3+} (in the high-spin state $t_{2g}^3e_g^1$) and Mn^{4+} ($t_{2g}^3e_g^0$) ions through the Mn – O – Mn bond chain.[7,8] A specific type of structural distortion of the perovskite lattice is realised owing to cooperative tilts and rotations of the MnO_6 octahedra, which is defined by the ratio of the radii of the cations in the sublattices A and B. Additionally, a deformation of the MnO_6 octahedra due to the Jahn – Teller effect (which is typical of Mn^{3+} cations in the high-spin electronic configuration) is superimposed on the cooperative distortion of the 3-dimensional framework. The situation can be further complicated if the deformation is static, *i.e.*, the

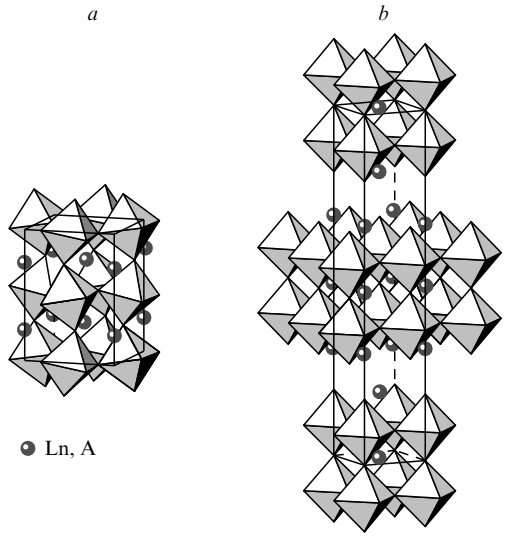


Figure 1. The crystal structures of $Ln_{1-x}A_xMnO_3$ (space group *Pnma*, $GdFeO_3$ structural type) (*a*) and $Ln_{2-x}A_{1+x}Mn_2O_7$ {$[(Ln,A)MnO_3]_n$.$[(Ln,A)O]$} (*b*).
Manganese atoms are in the centres of octahedra.

A M Abakumov, M G Rozova, E V Antipov Department of Chemistry, M V Lomonosov Moscow State University, Leninskie Gory, 119992 Moscow, Russian Federation. Fax (7-095) 939 09 98. Tel. (7-095) 939 52 44. E-mail: abakumov@icr.chem.msu.ru (A M Abakumov), rozova@icr.chem.msu.ru (M G Rozova). Tel. (7-095) 939 33 75. E-mail: antipov@icr.chem.msu.ru (E V Antipov)

Received 9 March 2004
Uspekhi Khimii **73** (9) 917 – 931 (2004); translated by Ya V Zubavichus

† Magnetoresistance is a change in the electrical resistance of a sample in an external magnetic field. Quantitatively, it is described by the magnetoresistive effect, which is given by the formula MR (%) = $100[(R_0 - R_H)/R_H]$, where R_0 and R_H are resistivities of the sample in the absence and in the presence of the external magnetic field with a strength H at a certain temperature, respectively. The term colossal magnetoresistance is applied to situations when the electrical resistivity changes in a magnetic field by a few orders of magnitude.

effect of orbital ordering takes place, and/or charge ordering occurs, being mainly observed at a doping level corresponding to the Mn^{3+} to Mn^{4+} ratio equal to unity (see Refs 9, 10). Nevertheless, a common feature of compounds $Ln_{1-x}A_xMnO_3$ is the retention of the spatial perovskite framework formed by vertex-sharing MnO_6 octahedra.

The discovery of colossal magnetoresistance in complex oxides $Ln_{2-x}A_{1+x}Mn_2O_7$ (Ln = La, Pr, Nd; A = Ca, Sr) stimulated studies of this phenomenon in other manganites with anisotropic layered structures.[11–15] The oxides $Ln_{2-x}A_{1+x}Mn_2O_7$ belong to the homologous series of the Ruddlesden–Popper phases with a general stoichiometry $A_{n+1}B_nO_{3n+1}$; their crystal structures may be described as intergrowth structures formed by regularly alternating perovskite and rock salt motifs, *i.e.*, $[(Ln,A)MnO_3]_n[(Ln,A)O]$ (Fig. 1 *b*). In terms of their electrical properties, the Ruddlesden–Popper phases are quasi-two-dimensional since conducting perovskite units (formed by vertex-sharing MnO_6 octahedra) are separted from each other by insulating blocks with the rock salt structure. These phases are convenient model objects for elucidation of the magnetic and electronic properties of complex manganites as a function of the dimensionality of the framework of the Mn–O–Mn bonds. Furthermore, the two-dimensional layered manganites represent a natural structural matrix suitable for the realisation of the colossal magnetoresistance by the mechanism of tunnelling of the conductivity electrons through the insulating blocks which separate the conducting perovskite fragments.

Complex manganites are similar to a certain extent to high-temperature superconducting (HTSC) cuprates as regards the possible formation of layered structures owing to the similarity in the crystal chemical properties of the cations Cu^{2+} and Mn^{3+}. Indeed, both cations are of the Jahn–Teller type due to partial filling of their e_g orbitals and thus it is a distorted octahedral environment (most often an axially elongated one) formed by oxygen atoms that is typical of them. The radii of octahedrally coordinated cations Cu^{2+} and Mn^{3+} (the latter being in the high-spin state) are also similar: $r(Mn^{3+}) = 0.79$ Å while $r(Cu^{2+}) = 0.87$ Å. Some of the axial oxygen atoms can be relatively easily removed from both the octahedrally coordinated Cu^{2+} and Mn^{3+} cations thus converting the coordination polyhedra into tetragonal pyramids. However, the square planar environment, which is often encountered in the structures of complex copper oxides, is not typical of manganese. Taking into account this close similarity, it is of no surprise that some layered perovskite-like complex manganese oxides have close analogues among HTSC cuprates. Perovskite and rock salt fragments are the major building blocks of layered cuprates as well. The known high-temperature superconducting cuprates $La_{2-x}A_xCuO_4$ (A = Sr, Ba) belong to the homologous series of the Ruddlesden–Popper phases $A_{n+1}B_nO_{3n+1}$ ($n = 1$) and have a structural analogue among manganites ($LaSrMnO_4$).[16, 17] A series of manganites including $Bi_{2-x}Pb_xSr_2MnO_{6+\delta}$ ($x = 0$, 1; the so-called 2201 phases)[18, 19] and $Bi_{2-x}Pb_xSr_{1.5}Ca_{1.5}Mn_2O_{9-\delta}$ (the 2212 phase) have been synthesised by analogy with the HTSC cuprates.[20] Another series of compounds with the composition $Bi_2Sr_2MnO_{6+\delta}$ (where δ is varied over a wide range), which correspond to an oxidation state of manganese in the range of $+2.7 < V_{Mn} < +3.3$ (see Ref. 21), have been prepared under high pressure.

The analogy between complex oxides of copper and manganese can be extended even further. According to one of the crystal chemical prerequisites to the formation of a layered perovskite-like structure with two different cations in the sublattice B, ordering of the cations is favoured by the difference in their coordination of oxygen atoms. The structure of brownmillerite $A_2BB'O_5$ represents a possible version of such a perovskite-derived layered structure. Formally, this anion-deficient structure is formed as a result of ordering of the anion vacancies giving rise to a regular alternation of the BO_2 and $B'O$ layers, which are characterised by the octahedral and tetrahedral coordination of the B and B′ cations, respectively (Fig. 2).

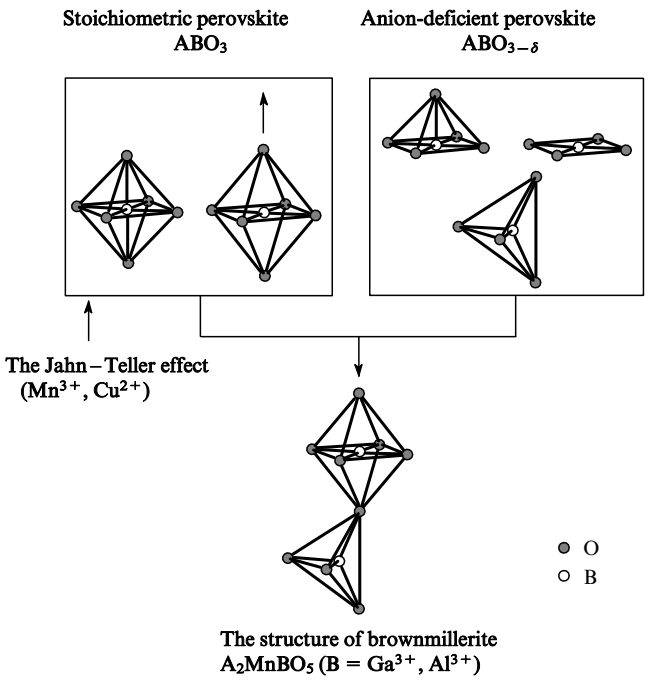


Figure 2. A scheme of formation and bonding of the coordination polyhedra BO_6 (an axially elongated octahedron) and $B'O_4$ (a tetrahedron) in the brownmillerite structure.

Since complex copper oxides with this structure are known, *viz.*, $LnACuGaO_5$ (Ln = La, Pr, Nd; A = Ca, Sr),[22–25] we have suggested that the synthesis of analogous manganese compounds is also possible. Taking into account different formal oxidation states of copper and manganese, the stoichiometry of manganites with the brownmillerite structure should be A_2MnGaO_5 ($V_{Mn} = +3$). An Al-containing analogue, *viz.*, Ca_2MnAlO_5, has been reported but it was considered only as a cement component rather than a potential magnetoresistant material.[26] An attractive feature of the brownmillerite structures as model objects in studies of magnetic and transport properties of layered manganites as a function of their composition and manganese oxidation state is its broad capability of 'tuning' changes in the anion stoichiometry and manganese valence. The preferable octahedral coordination of manganese atoms in oxidation states from +3 to +4 ensures retention of the perovskite-like MnO_2 layer whereas anion vacancies within the tetrahedral $B'O$ layers allow variations in the anion stoichiometry. The present review surveys different aspects of the synthesis of brownmillerites $A_2MnB'O_{5+\delta}$ (A = Ca, Sr; B′ = Ga, Al) and related compounds, their crystal structures and magnetic properties.

II. General information on the crystal structure of brownmillerites $A_2BB'O_5$

Brownmillerite $A_2BB'O_5$ is an anion-deficient analogue of perovskite ABO_3, which crystallises in the orthorhombic system and has unit cell parameters related to the unit cell parameter a_{per} of cubic perovskite as $a \approx \sqrt{2}a_{per}$, $b \approx 4a_{per}$, $c \approx \sqrt{2}a_{per}$. The structure of brownmillerite may be described as a result of regular alternation of the layers AO, BO_2 and $B'O$ along the unit cell axis *b* giving rise to the following layer sequence: BO_2–AO–$B'O$–AO–BO_2 (which constitutes half a repeat period along the *b* axis). The anion vacancies are ordered and localised in the $B'O$ layer, which can be formally produced from a perovskite $B'O_2$ layer (Fig. 3 *a*) by removal of half the oxygen atoms so as to form chains of anion vacancies going along the *a*

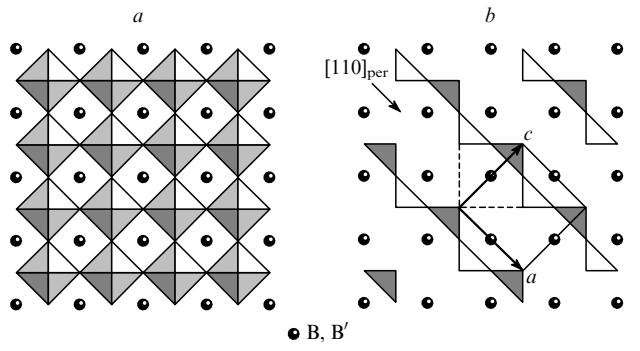


Figure 3. The structures of the BO_2 layers in the perovskite structure (*a*) and B′O layers in the structure of brownmillerite $A_2BB'O_5$ (*b*).
A cations are situated above and below the layer, the unit cell of perovskite is marked with dashes.

axis or, alternatively, along the [110] crystallographic direction of the parent perovskite (Fig. 3 *b*). The chains of vacant anion sites alternate with chains of sites occupied by oxygen atoms along the direction $c = [\bar{1}10]_{per}$. Owing to this ordered arrangement of anion vacancies, the coordination environment of the B′ cations is converted from octahedral to tetrahedral.

Thus, alternating layers of BO_6 octahedra and $B'O_4$ tetrahedra can be distinguished in the crystal structure of brownmillerite. The $B'O_4$ tetrahedra in the B′O layers are linked to each other through shared vertices to form chains along the *a* axis. The oxygen atoms in the B′O layers are shifted from their positions in the ideal cubic perovskite structure due to cooperative rotations of the tetrahedra in the chains around the *b* axis that is equivalent to the [001] direction of the parent perovskite (Fig. 4). As a result of the formation of the anion vacancies and cooperative shifts of oxygen atoms, the coordination number of the cations A (that are located between these layers) decreases from 12 to 8 + 2 (this notation means that two out of ten A−O bond lengths are substantially larger than the others).

The $B'O_4$ tetrahedra with opposite directions of rotation, *i.e.*, clockwise (CW) and counterclockwise (CCW), alternate along the chains of tetrahedra (see Fig. 4). These chains can adopt two configurations, *viz.*, left (L) and right (R), which are mirror reflections of each other.[27,28] If the vector $[\bar{1}10]_{per}$ translates a CW-tetrahedron of one chain into a CW-tetrahedron of another chain, both chains possess the same configuration (either L or R). On the contrary, if the vector $[\bar{1}10]_{per}$ translates a CW-tetrahedron of one chain into a CCW-tetrahedron of another chain or *vice versa*, these two chains possess different configurations. Mutual

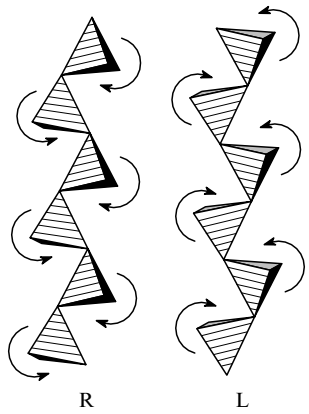


Figure 4. Chains of tetrahedra in the brownmillerite structure.
The arrows show directions of rotation of the respective tetrahedra.

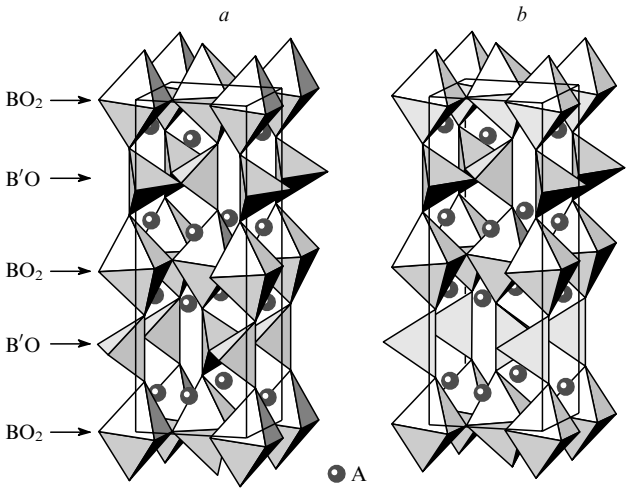


Figure 5. Crystal structures of two brownmillerite modifications with the space groups *I2mb* (*a*) and *Pnma* (*b*).

conversions of the L- and R-chains change neither the coordination polyhedra of the cations A, B and B′ nor respective interatomic distances since the space group of the parent perovskite includes the symmetry operations realising such conversions.[27,28] Hence, the L- and R-chains should be energetically equivalent and with similar probabilities of their formation.

For the majority of brownmillerites, three variants of space symmetry, which correspond to different ways of ordering the chains of tetrahedra belonging to the two configurations, are considered. In the case of completely random arrangement of the L- and R-chains, the structure belongs to the space symmetry group *Imma*. If only one type of chain is present, the structure belongs to the noncentrosymmetrical group *I2mb* (Fig. 5 *a*). Regular alternation of the B′O layers formed exclusively by either L- or R-chains gives rise to the space group *Pnma* (Fig. 5 *b*). However, the pattern of ordering of the chains of tetrahedra can be more complicated than the above three variants. Ordering of the L- and R-chains of tetrahedra can occur within one B′O layer thus increasing the repeat period along the *c* axis. Superstructural reflections corresponding to the regular alternation of the chains of tetrahedra along this axis have indeed been observed for brownmillerites such as Sr_2CuGaO_5,[29] $Ba_2In_2O_5$ [30] as well as for related phases $LnSr_2GaCu_2O_7$ (where Ln is a rare-earth element, the so-called Ga1212 phases), which contain GaO layers with brownmillerite-like chains of tetrahedra.[27,28]

A unified model encompassing all types of such superstructural ordering has been proposed by Lambert *et al.*[31] According to this model, the brownmillerite structure may be regarded as a lattice commensurately modulated with respect to the starting orthorhombic unit cell (with the unit cell parameters $a \approx \sqrt{2}a_{per}$, $b \approx 4a_{per}$ and $c \approx \sqrt{2}a_{per}$) by a modulation vector $\boldsymbol{q} = \gamma c^*$ giving rise to the (3 + 1)-dimensional space group $Imma(00\gamma)s00$.‡ In this case, the pattern of alternation of the chain of tetrahedra in the structure can be unambiguously described by a step function of the occupancy modulation. This function is defined in (3 + 1)-dimensional space by an interval on the a_4 axis with a width $\Delta(x_4)$ centred at x_4^0. An atom is assigned an occupancy of 1 if its x_4 coordinate lies inside the interval Δ, while an occupancy of 0 is assigned if the coordinate lies beyond it. In order to determine the widths and centres of the intervals defining the step functions of the occupancy modulation, it is necessary to apply the symmetry operations of the (3 + 1)-dimensional space group $Imma(00\gamma)s00$

‡ Fundamentals of space groups with the dimensionality > 3 as applied to description of modulated structures (supplied with a detailed reference list) are given in the International Tables for Crystallography.[32]

to all oxygen atoms in the B′O layer taking into account that the change in the configuration of a chain of tetrahedra should not change the composition of the layer or result in defects in the sequential arrangement of tetrahedra along the chain. For a cross-section of the brownmillerite structure on the $(x, 1/4, z)$ plane, which corresponds to the plane of the B′O layer, the sequence of atoms O*a*–Ga1–O*c*–Ga1 corresponds to the R-chain of tetrahedra, while the sequence Ga2–O*b*–Ga2–O*d* corresponds to the L-chain (Fig. 6). Since only one chain can be present in a specific point of the crystal lattice, the interval width Δ of the step function is equal to 1/2 for all atoms in this layer. The atoms O*a* and O*c* belong to the same chain of tetrahedra and thus they should be present in the structure simultaneously. Phases of the step function for these atoms should be equal, *i.e.*, $t(\mathrm{O}a) = t(\mathrm{O}c)$. This gives rise to the following relation between the coordinate t of the centre of the step function domain and the γ component of the modulation vector (see Fig. 6 for the case of $\gamma = 1/2$).

$$t = \frac{1-\gamma}{4}.$$

Taking into account that $t = x_4 - \boldsymbol{q}\,\boldsymbol{r}_{\mathrm{av}}$ (where $\boldsymbol{r}_{\mathrm{av}}$ is a vector defining the position of an atom in the average structure), the coordinate x_4^0 of the domain centre for the chain O*a*–Ga1–O*c*–Ga1 is given by

$$x_4^0(\mathrm{R}) = \frac{1-\gamma}{4} + \gamma z\,.$$

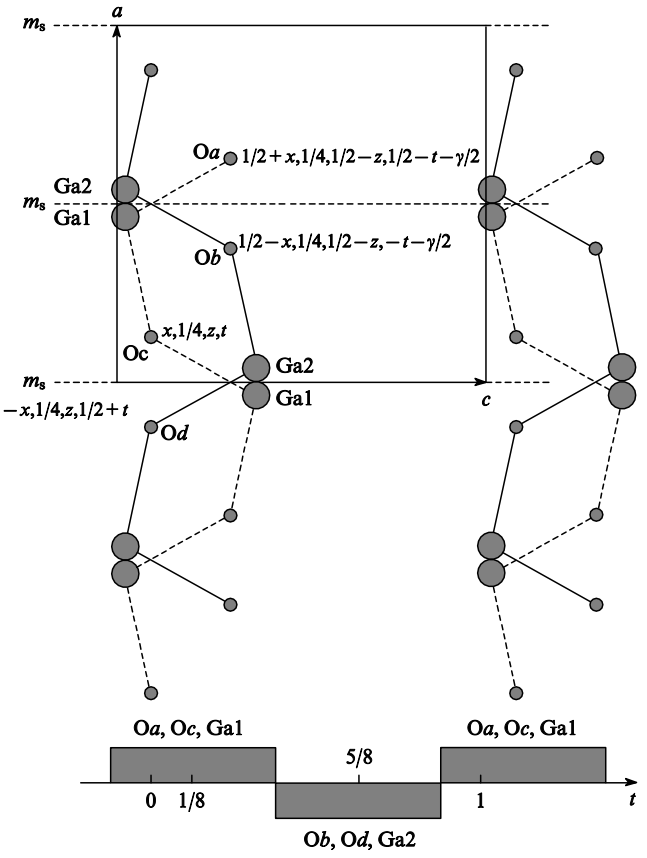


Figure 6. Arrangements of atoms in the B′O layer $(x, 1/4, z)$ for R- and L-chains of tetrahedra.
The sequence O*a*–Ga1–O*c*–Ga1 (dashed line) corresponds to the R-chain; the sequence Ga2–O*b*–Ga2–O*d* (solid line) corresponds to the L-chain; for the oxygen atoms, four-dimensional coordinates (x, y, z, t) are given; the positions of domains of the step function of the occupancy modulation are given for $\gamma = 1/2$.

The chain Ga2–O*b*–Ga2–O*d* is symmetrically related to the chain O*a*–Ga1–O*c*–Ga1 through a mirror plane m_s, which shifts the modulation phase by 1/2

$$x_4^0(\mathrm{L}) = \frac{1-\gamma}{4} + \gamma z + 1/2\,,$$

i.e., since $\Delta(x_4) = 1/2$, the two chains cannot be present at the same point of the crystal structure simultaneously. A translation by one repeat period of the parent structure along the *c* axis (*i.e.*, between two neighbouring chains in the layer) shifts the modulation phase by γ. Therefore, the sequence of alternation of the L- and R-chains can be unambiguously defined by the γ component of the modulation vector. This model is applicable for any values of the γ component. The three-dimensional symmetry group of a specific structure can be derived from the symmetry operations of the (3+1)-dimensional space group *Imma*(00γ)*s*00 for any rational γ and initial phase t of the modulation (Table 1).[31] As is clearly seen from Table 1, the brownmillerite structures with the space groups *I*2*mb* and *Pnma* correspond to two limiting cases, *viz.*, $\gamma = 0$ and $\gamma = 1$.

Table 1. Three-dimensional space groups corresponding to the brownmillerite structures with the modulation vector $\boldsymbol{q} = \gamma c^*$, (3+1)-dimensional space group *Imma*(00γ)*s*00 and different possible combinations of γ and t (r, s, v, τ, μ are integers).

$\gamma = r/s$ ($r < s$)	Space group at		
	$t = v/2s$	$t = (2v+1)/4s$	other t
$\gamma = 0$	*I*2*mb*	*I*2*mb*	*I*2*mb*
$r = 2\tau$, $s = 2\mu + 1$	$I2_1/m$	*I*2*mb*	*Im*
$r = 2\tau + 1$, $s = 2\mu + 1$	*Pnma*	*Pnmb*	$Pnm2_1$
$s = 2\mu$	*Pcmb*	*Pcma*	$Pcm2_1$
$\gamma = 1$	*Pnma*	*Pnmb*	$Pnm2_1$

The crystal structure of brownmillerite is a suitable matrix to accomodate the Jahn–Teller cations in its octahedral sites. A common feature of brownmillerites contaning transition metals is the elongation of two axial B—O distances in the BO_6 octahedra as compared to four equatorial distances. This distortion is due to alternation of the vertex-sharing BO_6 octahedra and $B'O_4$ tetrahedra along the *b* axis rather than to the electronic structure of the B cation. Since the B′—O distances are shorter than the B—O distances owing to the smaller coordination number, a decrease in the $B'-O_{ax}$ bond length has to be compensated by the respective elongation of the $B-O_{ax}$ bond. In fact, axial distortions of the BO_6 octahedra are observed not only for cations manifesting the Jahn–Teller effect, such as Cu^{2+}, but also for cations devoid of this property (Table. 2). Brownmillerites contaning Fe^{3+} (electronic configuration d^5) may serve as an example. Filling an octahedral cavity with a Jahn–Teller cation favours the formation of the brownmillerite structure owing to stabilisa-

Table 2. The B—O bond lengths (B = Cu, Fe) in copper- and iron-containing brownmillerites.

Oxide	$d(B-O_{eq})$ /Å	$d(B-O_{ax})$ /Å	Ref.
$LaCaCuGaO_5$	1.916–1.922	2.406	24, 25
$LaSrCuGaO_5$	1.888–1.934	2.436–2.478	22, 23
$PrSrCuGaO_5$	1.731–2.112	2.494	23
$NdSrCuGaO_5$	1.913–1.930	2.407–2.409	23
$Ca_2Fe_2O_5$	1.957–1.970	2.114–2.130	33–35
$Sr_2Fe_2O_5$	1.940–2.028	2.202–2.217	36, 37
Ca_2FeAlO_5	1.942–1.954	2.217	38
Ca_2FeGaO_5	1.954–1.959	2.128	39

tion of a distorted octahedral environment. Therefore, possible retention of the oxidation state +3 for the manganese cations should be taken into account when selecting a method for the synthesis of Mn-containing brownmillerites.

III. Synthesis of Mn-containing brownmillerites

The ceramic method is typically applied for the synthesis of Mn-containing brownmillerites $A_2MnB'O_5$ (A = Ca, Sr; B′ = Ga, Al). The temperature and partial pressure of oxygen at which the solid-state reaction is performed strongly influence the phase composition of the reaction products and degree of ordering of the manganese and B′ cations over octahedral and tetrahedral sites. Monophasic $Ca_2MnB'O_5$ with fully ordered manganese and B′ cations (according to the neutron diffraction data) is obtained in a ceramic synthesis starting from $CaCO_3$, manganese oxides (Mn_2O_3, MnO_2) or manganese oxalate and B'_2O_3 oxides conducted at 1200–1250 °C in a flow of an inert gas (N_2).[40,41] Synthesis of the same products in air requires higher temperatures (1300–1350 °C) in order to stabilise the phase at elevated partial oxygen pressure. An analysis of IR spectra of Ca_2MnAlO_5 suggested that an increase in the temperature of the synthesis favours partial disordering of the manganese and aluminium cations.[26] When the synthesis of Ca_2MnGaO_5 is performed in air at 1300 °C, a perovskite phase (presumably with disordered positions of manganese and gallium cations) is formed as an admixture.[40] Disordering of these cations (up to 5% of the Mn cations occupy Ga positions) is also observed in the synthesis of Sr_2MnGaO_5 at 1350 °C in a flow of nitrogen.[41,42] Meanwhile, $SrCaMnGaO_5$ with the fully ordered structure can be prepared at 1200 °C in a flow of argon.[43]

Taking all the above data into account, one may conclude that the formation of the ordered layered brownmillerite structure is favoured by a decrease in the temperature of the solid-state reaction and in the partial oxygen pressure. The latter is necessary to preserve the formal +3 oxidation state of the manganese cations and the overall anion stoichiometry, which should be identical or close to the nominal stoichiometry of brownmillerite, *i.e.*, $A_2MnB'O_5$ [this makes it possible to utilise differences in the coordination environment of the manganese (octahedral) and B′ (tetrahedral) cations to stabilise the ordered layered phase]. For instance, an increase in the coordination number of the B′ cations to 6 gives rise to disordered perovskite phases with a three-dimensional framework of octahedra despite the retention of the manganese oxidation state $V_{Mn} = +3$. In particular, the compounds Ln_2MnGaO_6 (Ln = La, Nd) are characterised by an orthorhombic structure (which belongs to the structural type of $GdFeO_3$) with manganese and gallium cations statistically occupying octahedral sites.[44,45] A similar situation was revealed for solid solutions with a common stoichiometry $La_{2-x}Sr_xMnGaO_6$ ($x = 0.7$), which crystallise in the monoclinic system (sp. gr. $I2/c$) and are characterised by an oxidation state of manganese other than +3.[46,47] A change in the Mn/Ga stoichiometric ratio also prevents formation of the layered brownmillerite structure. Solid solutions $SrMn_{1-x}Ga_xO_{3-\delta}$ ($0 \leqslant x \leqslant 0.33$) have a disordered cubic perovskite structure whereas for $0.33 < x < 0.5$, a two-phase region was found.[48]

We have suggested that the optimum conditions for the formation of brownmillerites Ca_2MnGaO_5 and Sr_2MnGaO_5 could be achieved provided that the synthesis is performed in evacuated sealed quartz tubes starting from CaO (SrO) preformed by decomposition of the respective carbonates in a dynamic vacuum (10^{-2} mbar, 900 °C), Mn_2O_3 and Ga_2O_3. The use of highly reactive oxides of alkaline-earth metals at a low partial oxygen pressure in the tube allows the preparation of monophasic ordered brownmillerites at 1000 °C.[40,49,50] The samples containing alkali-metal oxides have to be handled in a glove box free of water vapour and CO_2.

Brownmillerites containing manganese in an oxidation state slightly above +3 can be prepared by the heterovalent substitution of a bivalent cation for a trivalent one in the B′ sublattice. A series of solid solutions $Ca_2MnGa_{1-x}Zn_xO_{5+\delta}$, where $x = 0.1$ ($\delta = 0.075$, $V_{Mn} = +3.25$) or $x = 0.2$ ($\delta = 0.08$, $V_{Mn} = +3.36$) have been synthesised; phases with an increased manganese oxidation state are formed when the synthesis is performed at 1200 °C in air.[40] The manganese atoms in the original brownmillerite $Ca_2MnGaO_{5+\delta}$ with $\delta = 0$ can be further oxidised by annealing at low temperature and high partial oxygen pressure. Insertion of oxygen into this compound proceeds under drastic conditions ($T = 415$ °C, $p_{O_2} = 80$ atm); no complete oxidation of manganese to $V_{Mn} = +4$ occurs, the maximum reachable value of δ is 0.39.[40] Annealing $Sr_2MnGaO_{5+\delta}$ under milder conditions ($T = 415$ °C, $p_{O_2} = 1-20$ atm) gives rise to almost complete oxidation to $\delta = 0.47-0.505$. $Sr_2MnGaO_{5+\delta}$ with an intermediate value of the oxygen overstoichiometry index $0 < \delta < 0.5$ can be prepared by reduction of fully oxidised $Sr_2MnGaO_{5.5}$ in a closed circuit with a preset partial oxygen pressure.[51] In this method, the annealing is performed in a circulating flow of an argon–oxygen mixture; the required partial oxygen pressure is kept constant using a Cu/Cu_2O getter and controlled by an electrochemical cell with a solid oxygen-ionic electrolyte. A series of phases with $\delta = 0.13$ ($\log p_{O_2} = -5.19$), $\delta = 0.41$ ($\log p_{O_2} = -4.04$) and $\delta = 0.46$ ($\log p_{O_2} = -1.12$) have been synthesised at 415 °C using this method. A biphasic region corresponding to a mixture of a reduced and an oxidised phase with $\delta = 0.13$ and 0.41, respectively, was observed in the range of $0.13 < \delta < 0.41$.

IV. The crystal structure of $A_2MnB'O_{5+\delta}$ (A = Ca, Sr; B′ = Ga, Al; $\delta \approx 0$)

Unit cell parameters and space groups of Mn-contaning brownmillerites corresponding to different oxygen overstoichiometry indices are listed in Table 3. Based on X-ray powder diffraction data,[26] a primitive orthorhombic unit cell was suggested for Ca_2MnAlO_5. A subsequent low-temperature neutron diffraction study of this phase has given the space group $I2mb$.[41] For the Ga-containing analogue, *i.e.*, $Ca_2MnGaO_{5.045}$, formation of the *Pnma* modification of brownmillerite was unambiguously established by electron diffraction and X-ray powder diffraction.[40] Refinement of the crystal structure of $Ca_2MnGaO_{5.045}$ within the *Pnma* model using the Rietveld method resulted in a good correspondence between the experimental and calculated X-ray powder diffraction patterns.

Nevertheless, the real structure of $Ca_2MnGaO_{5.045}$ proved to be much more complicated than the idealised *Pnma* model, as evidenced by neutron diffraction and high-resolution electron microscopy (HREM). While the *Pnma* model provides a reasonable description of the experimental X-ray diffraction pattern, the neutron diffraction pattern can be fitted within this model only with large reliability factors. Systematic underestimation of the calculated intensities of reflections with $h + k + l = 2n$ and a nonmonotonic dependence of the FWHMs of reflections on the interplanar distance indicate the co-existence of two brownmillerite polymorph modifications with the space groups *Pnma* and *I2mb* in the sample. If the *I2mb* phase is taken into account in the fitting procedure, the fit quality is significantly improved. However, the Fourier difference maps for the *Pnma* phase still reveal extra maxima corresponding to incomplete ordering of the chains of tetrahedra (89% of one type of chain and 11% of another type within one layer instead of 100% of a certain type of chain, which has to be observed in the case of the ideal *Pnma* model). These results of structure refinement using neutron diffraction data can be interpreted as indicating the simultaneous presence of the *Pnma* and *I2mb* domains in the crystal structure of $Ca_2MnGaO_{5.045}$. The HREM data fully support this model.[40] Figure 7 shows two HREM micrographs of $Ca_2MnGaO_{5.045}$ along the crystallographic direction [101] and their Fourier images corresponding to the *Pnma* and *I2mb* phases. Reflections of the hkl, $k \neq 2n$ type are clearly resolvable in Fig. 7 *a* but absent in Fig. 7 *c*, so that the

Table 3. The crystallographic data for brownmillerites $A_2MnB'O_{5+\delta}$ (A = Ca, Sr; B′ = Ga, Al).

Composition	Unit cell parameters /Å			Space group	Oxygen overstoichiometry index		T /K	Ref.
	a	b	c		value	method [a]		
$Ca_2MnAlO_{5+\delta}$	5.244(2)	14.904(2)	5.465(1)	see [b]	–		293	26
	5.23135(8)	14.9533(3)	5.46258(9)	*I2mb*	0	TGA, ND	2	41
$Ca_2MnGaO_{5+\delta}$	5.2685(4)	15.301(1)	5.4686(5)	*Pnma*	0.045	CA, ND	293	40
	5.2712(7)	15.267(1)	5.4722(6)	*Pnma*	0.09	CA	293	40
	5.302(1)	14.940(4)	5.428(2)	*Pnma*	0.39	CA	293	40
$Ca_2MnGa_{0.9}Zn_{0.1}O_{5+\delta}$	5.278(1)	15.216(4)	5.479(1)	*Pnma*	0.075	CA	293	40
$Ca_2MnGa_{0.8}Zn_{0.2}O_{5+\delta}$	5.278(1)	15.163(5)	5.486(1)	*Pnma*	0.08	CA	293	40
$SrCaMnGaO_{5+\delta}$	5.3196(2)	15.7817(6)	5.4925(2)	*I2mb*	0.035	CA, ND	290	43
	5.30562(6)	15.7705(2)	5.48090(7)	*I2mb*	0.035	CA, ND	2	43
$Sr_2MnGaO_{5+\delta}$	5.4023(5)	16.130(2)	5.5645(7)	*I2mb, Imma*	−0.03	CA	293	51
	5.3717(6)	16.234(2)	5.5033(6)	*Imma*	0	TGA	293	42
	5.35450(2)	16.2256(6)	5.4888(2)	*Imma*	0	TGA, ND	2	41
	5.3863(1)	16.1971(3)	5.5257(1)	*I2mb, Imma*	0.01	CA, ND	293	52
	5.3894(4)	16.193(1)	5.5348(4)	*Imma*	0.025	CA	293	51
	5.3700(5)	16.240(2)	5.4976(4)	*Imma*	0.13	CA	293	51
	5.3628(3)	8.0193(8)	5.4066(3)	*Bmmm*	0.41	CA	293	51
	5.3666(6)	7.959(2)	5.3861(5)	*Bmmm*	0.46	CA	293	51
	3.7995(1)	–	7.9209(3)	*P4/mmm*	0.505	CA	293	51
	5.3834(2)	5.3652(2)	7.9448(2)	*Cmmm*	0.5	TGA, ND	293	48

[a] TGA stands for thermogravimetric analysis, ND stands for neutron diffraction, CA stands for chemical analysis. [b] Primitive orthorhombic lattice.

apparent repetition period along the b axis for the *I2mb* phase appears half as long as that for the *Pnma* phase (b = 15.3 Å).

In addition to crystallites strictly corresponding to one of the two variants (either *Pnma* or *I2mb*), the HREM data revealed crystallites with narrow extended domains of the *I2mb* phase embedded into the *Pnma* matrix. Thus, the real structure of $Ca_2MnGaO_{5.045}$ represents a mixture of the polymorph modifications *Pnma* and *I2mb*, both at the level of separate crystallites (which manifests itself in the structure refinement using neutron diffraction data as a contribution from the *I2mb* phase) and narrow domains within one crystallite (which manifests itself in the neutron diffraction data as the presence of differently oriented chains within the *Pnma* phase).

Substitution of strontium atoms for calcium in $Ca_2MnGaO_{5+\delta}$ suppresses formation of the *Pnma* modification. The crystal structure of $SrCaMnGaO_{5.035}$ was successfully refined using neutron diffraction data within the fully ordered *I2mb* model.[43] A similar model was applied to refine the structure of $Sr_2MnGaO_{5+\delta}$ ($\delta < 0$) from X-ray[49] and neutron powder diffraction data.[52, 53] However, it was found that it is the *Imma* structural model with a disordered arrangement of the L- and R-chains of tetrahedra that better reproduces the neutron diffraction pattern for Sr_2MnGaO_5. The difference between the fit qualities obtained for this compound within the *I2mb* and *Imma* models is not as significant as in the case of Ca_2MnAlO_5.[41, 52] This can be seen from a comparison of the corresponding integral discrepancy factors χ^2 (see Ref. 41):

Oxide	Sr_2MnGaO_5	Sr_2MnGaO_5	Ca_2MnAlO_5	Ca_2MnAlO_5
Sp. gr.	*Imma*	*I2mb*	*Imma*	*I2mb*
χ^2	3.30	5.28	27.5	2.99

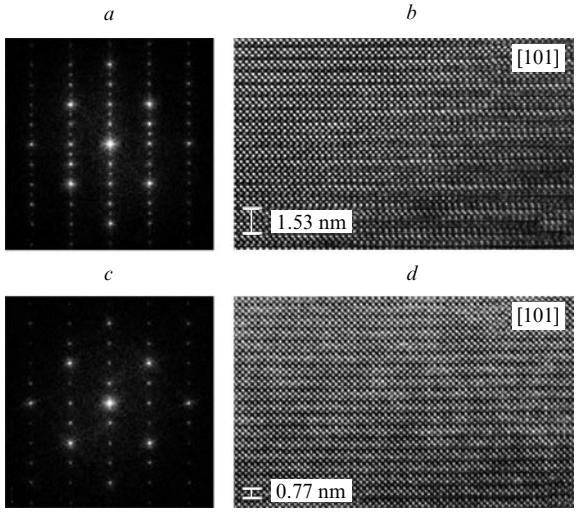


Figure 7. HREM micrographs (a, c) and respective Fourier images for $Ca_2MnGaO_{5.045}$ along the crystallographic direction [101] (b, d) showing domains of the *Pnma* (a, b) and *I2mb* (c, d) phases.

Actually, the ordering of the chains of tetrahedra in Sr_2MnGaO_5 has a more complicated character as compared with the idealised *I2mb* and *Imma* models. An electron diffraction study of Sr_2MnGaO_5 has revealed superstructural reflections corresponding to ordering of the L- and R-chains in the GaO layers along the axis c.[54] These reflections can be indexed assuming a modulation vector of $\boldsymbol{q} = (1/2)c^*$, which corresponds to a sequence of alternating chains of tetrahedra L–R–L–R–L along the c axis according to the Labmert model (see section II). Alternatively, this structure can be described in the orthorhombic space group *Pcmb* with a doubled c parameter (Fig. 8). This model was confirmed using HREM.[54] In addition to the regularly ordered fragments of the *Pcmb* phase, domains with another type of shift of the ordered layers of tetrahedra, which corresponded to a monoclinic unit cell (a = 17.100 Å, b = 5.406 Å, c = 11.118 Å, β = 108.97°, sp. gr. $P2/c$) (Fig. 9), were revealed together with numerous defects due to disturbed alternation sequences of the L- and R-chains of tetrahedra.

These two examples, *viz*., $Ca_2MnGaO_{5+\delta}$ and $Sr_2MnGaO_{5+\delta}$ demonstrate that structural analysis of brownmillerite phases can become very complicated due to the multitude of ordering patterns of the chains of tetrahedra. Even neutron powder diffraction, which is quite sensitive to the positions of oxygen atoms, is often insufficient to determine the real structure of brownmillerites and thus it should be applied in a combination

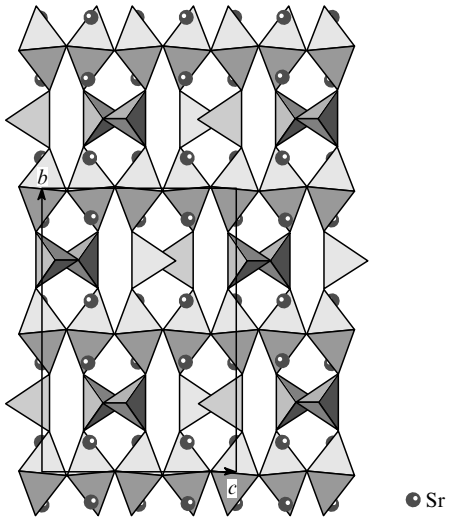


Figure 8. A model of the crystal structure of Sr_2MnGaO_5 with the chains of tetrahedra ordered according to the L – R – L – R pattern.
The two different projections of the GaO_4 tetrahedra correspond to the two chain types.

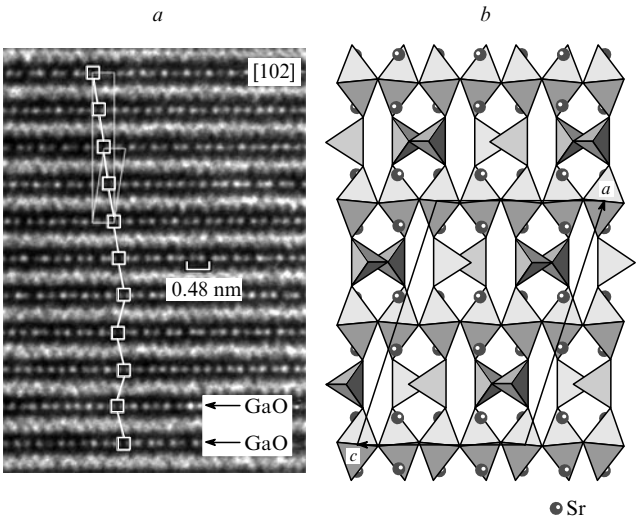


Figure 9. HREM micrographs of defects in the structure of Sr_2MnGaO_5 (*a*) and a model of this structure in the monoclinic space group $P2/c$ (*b*).

with local diffraction methods, *e.g.*, electron diffraction as implemented in transmission electron microscopes and HREM. High-temperature electron diffraction makes it possible to determine the influence exerted by the synthesis and annealing conditions on the character of ordering of the chains of tetrahedra. The electron diffraction patterns for the [010]* zone of Sr_2MnGaO_5 in the temperature range from room temperature to ~900 °C are shown in Fig. 10.[54] It is clearly seen that at 620 °C, the intensity of satellite reflections corresponding to the superstructure $\boldsymbol{q} = (1/2)c^*$ decreases and stripes of diffuse scattering oriented along the c^* axis appear. At 665 °C, the satellites completely disappear while the stripes of diffuse scattering remain, which suggests the loss of long-range ordering in the arrangement of the chains of tetrahedra at this temperature. Ordering is completely destroyed at ~900 °C (Fig. 10 *d*). This temperature is lower than the minimum temperature required for the synthesis of Mn-containing brownmillerites (1000 °C). This means that specific ordering of the chains of tetrahedra is realised not at the temperature of the synthesis of the sample but rather during its subsequent cooling. Hence, the exact character of the ordering should depend on the cooling rate.

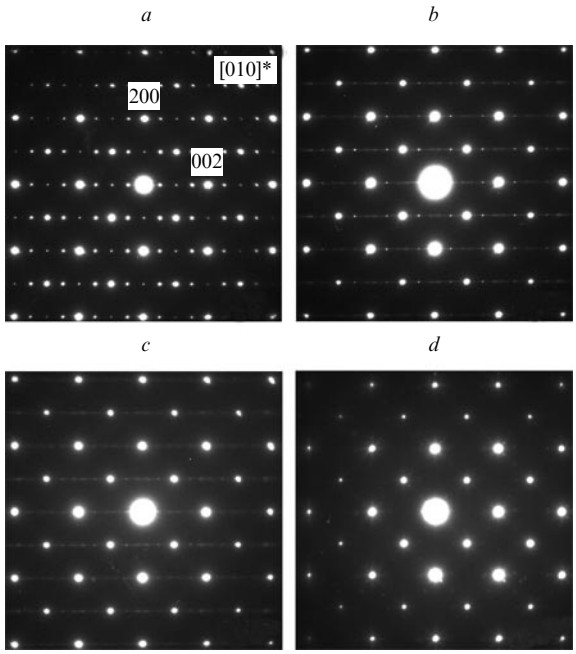


Figure 10. Electron diffraction patterns for the [010]* zone of Sr_2MnGaO_5 at room temperature (*a*), 620 °C (*b*), 665 °C (*c*) and 905 °C (*d*).

All brownmillerites $A_2MnB'O_{5+\delta}$ (A = Ca, Sr; B′ = Ga, Al; $\delta \approx 0$) are characterised by strong distortions of the MnO_6 octahedra. The lengths of the equatorial and axial Mn – O bonds for various members of this family, as determined by neutron diffraction, are listed in Table 4. A direct comparison of the bond lengths would not be informative since the respective values were determined for compounds with different oxygen content at different temperatures. However, a tendency that two axial Mn – O bonds are substantially longer than four equatorial ones is apparent for all the structures. Such a deformation of the coordination polyhedron is typical of the Jahn – Teller high-spin Mn^{3+} cation with the electronic configuration $t_{2g}^3e_g^1$. It is of note that the length of an axial Mn – O bond depends on the mean radius of cations in the sublattice A: it increases from 2.239 Å for A = Ca to 2.308 Å for A = Sr, Ca and further to 2.368 Å for A = Sr. As will be shown below, the bond length is also dependent on the oxidation state of manganese.

Table 4. The Mn – O bond lengths in the structures of brownmillerites $A_2MnB'O_{5+\delta}$ (A = Ca, Sr; B′ = Ga, Al) with $\delta \approx 0$.

Composition	d(Mn – O)$_{eq}$ /Å	d(Mn – O)$_{ax}$ /Å	δ	T/K	Ref.
$Ca_2MnAlO_{5+\delta}$	1.888(2) × 2	2.249(1) × 2 1.909(2) × 2	0	2	41
$Ca_2MnGaO_{5+\delta}$	1.899(4) × 2 1.918(4) × 2	2.239(3) × 2	0.045	293	40
$SrCaMnGaO_{5+\delta}$	1.890(6) × 2 1.941(6) × 2	2.308(2) × 2	0.035	290	43
	1.888(6) × 2 1.932(6) × 2	2.299(2) × 2	0.035	2	43
$Sr_2MnGaO_{5+\delta}$	1.9302(1) × 4	2.368(3) × 2	0.01	293	52
	1.91872(7) × 4	2.375(1) × 2	0	2	41

V. Specific pattern of the oxidation of brownmillerites $A_2MnGaO_{5+\delta}$ (A = Ca, Sr)

An increase in the formal oxidation state of manganese in $A_2MnGaO_{5+\delta}$ as a result of a heterovalent substitution in the cation sublattice or insertion of oxygen atoms converts the electronic configuration of Mn from $t_{2g}^3e_g^1$ to $t_{2g}^3e_g^0$ and is accompanied by a suppression of the Jahn–Teller effect and decrease in the axial Mn–O bond lengths in the MnO_6 octahedra. In the case of $Ca_2MnGaO_{5+\delta}$ and solid solutions based on it, these bond lengths decrease monotonically with an increase in the oxidation state of manganese (V_{Mn}).[40, 55]

Oxide	$Ca_2MnGaO_{5.045}$	$Ca_2MnGa_{0.8}Zn_{0.2}O_{5.08}$	$Ca_2MnGaO_{5.39}$
V_{Mn}	+3.09	+3.36	+3.78
d(Mn–O) /Å	2.239(3)	2.221(9)	1.873(9)

In the latter compound, the MnO_6 octahedra are axially compressed (*i.e.*, the axial Mn–O bonds are shorter than the equatorial ones). Since the axial Mn–O bonds are oriented nearly parallel to the *b* axis, their contraction results in a decrease in the *b* parameter of the unit cell. In the case of $Ca_2MnGaO_{5+\delta}$ and $Ca_2MnGa_{1-x}Zn_xO_{5+\delta}$, the *b* *vs.* V_{Mn} function is nearly linear (Fig. 11). Therefore, the *b* parameter is sensitive to changes in the oxidation state of manganese. The range of oxygen nonstoichiometry possible for Ca_2MnAlO_5 has not been studied, however, one may assume that this compound can be characterised by variable oxygen content, since the *b* parameter for a sample prepared in air [26] is significantly smaller than the respective value for a sample prepared in an inert atmosphere,[41] which assumes that the oxidation state is higher for the products synthesised in air.

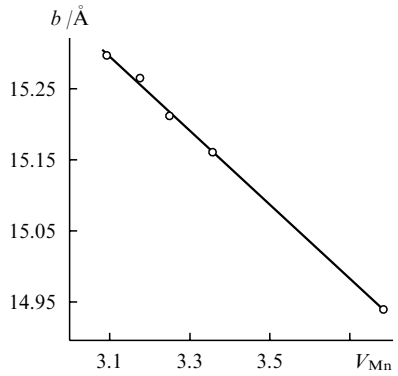


Figure 11. Changes in the *b* parameter as a function of V_{Mn} for $Ca_2MnGaO_{5+\delta}$ and $Ca_2MnGa_{1-x}Zn_xO_{5+\delta}$.

A heterovalent substitution of Zn for Ga leads to a substantial change in the *b* parameter alone while the *a*, *c* parameters and the degree of the orthorhombic distortion of the unit cell change insignificantly, mainly due to variation of the mean radii of cations occupying B and B′ positions. On the contrary, insertion of excess oxygen (*i.e.*, an increase in the index δ) gives rise to a significant decrease in the degree of the orthorhombic distortion, which is reflected in an increase in the *a* parameter coupled with a decrease in the *c* parameter (see Table 3). This occurs because the geometry of a part of the anion-deficient $GaO_{1+\delta}$ layers changes when extra oxygen atoms appear. An electron diffraction and HREM study has shown that insertion of oxygen into the $Ca_2MnGaO_{5+\delta}$ structure proceeds inhomogeneously.[40] Oxidation affects only half of the anion-deficient GaO layers giving rise to an ordered arrangement of GaO_2 and GaO□ (□ is the anion vacancy) (Fig. 12). The idealised structure of the oxidised material can be represented by the following layer sequence:

$GaO_2–CaO–MnO_2–CaO–GaO□–CaO–MnO_2–CaO–GaO_2$,

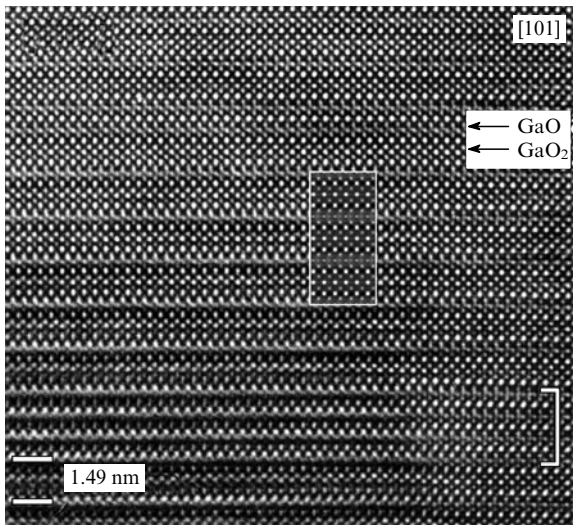


Figure 12. HREM micrographs of $Ca_2MnGaO_{5.39}$ along the crystallographic direction [101].
The square bracket shows a domain of the starting reduced phase with the *I2mb* structure, the inset in the centre shows an image calculated theoretically for the $Pmc2_1$ model.

two adjacent Ga layers are not symmetrically related to each other. Such a structure can be described in the noncentrosymmetrical space group $Pmc2_1$, which is actually a noncentrosymmetrical subgroup of the group *Pnma*. The resultant unit cell parameters relate to the unit cell parameters of the original cubic perovskite as $a \approx 4a_{per}$, $b \approx c \approx \sqrt{2}a_{per}$. The ordered disposition of the GaO□ and GaO_2 layers is violated by the slabs of the starting reduced phase with the *I2mb* structure. The structure of a completely oxidised compound is described by an idealised formula $Ca_2MnGaO_{5.5}$ [$Ca_4(Mn_2Ga)GaO_{11}$], which corresponds to the third member of the homologous series of the brownmillerite structures $A_{n+1}B_nB'O_{3n+2}$ (n = 3, Fig. 13). In this structure, triple layers of BO_6 octahedra (B = Mn, Ga) are separated by a layer of $B'O_4$ tetrahedra (B′ = Ga). According to the above stoichiometry, the oxidation state of manganese in these fragments should be +4, however the mean oxidation state of manganese was +3.78 in a sample oxidised at p_{O_2} = 80 atm due to the presence of areas with the original *I2mb* structure corresponding to $V_{Mn} \approx +3$. Probably, the phase with the ideal

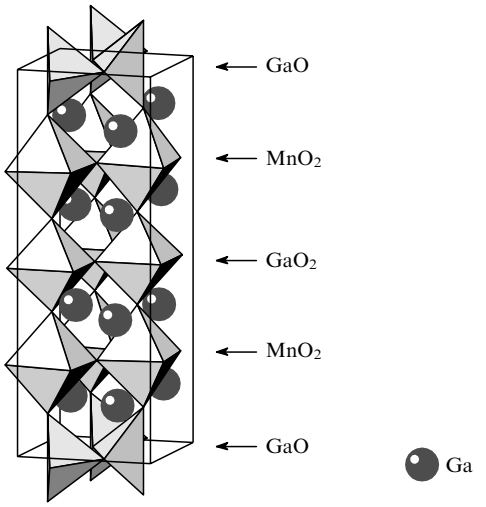


Figure 13. A model of the crystal structure of a completely oxidised phase $Ca_2MnGaO_{5.5}$.

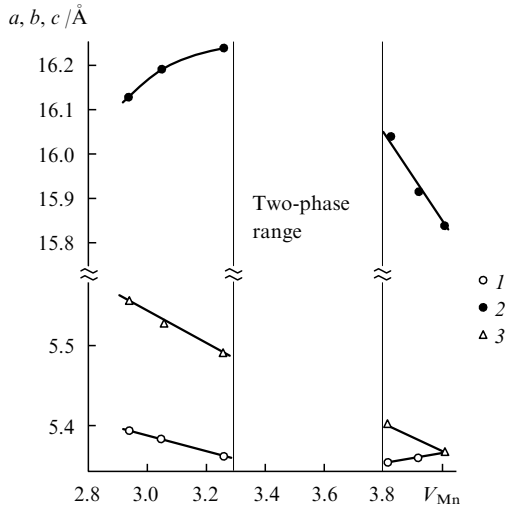


Figure 14. Changes in the unit cell parameters *a* (*1*), *b* (*2*) and *c* (*3*) as a function of the manganese oxidation state in $Sr_2MnGaO_{5+\delta}$.

stoichiometry $Ca_2MnGaO_{5.5}$ can be prepared at a higher partial oxygen pressure and longer duration of annealing.

The oxide $Sr_2MnGaO_{5+\delta}$ is characterised by a more complex dependence of the unit cell parameters on the oxidation state of manganese V_{Mn} and oxygen content.[51,56] The unit cell volume, degree of its orthorhombic distortion and *c* parameter decrease regularly with an increase in δ (Fig. 14, see Table. 3). The *a* and *b* parameters behave differently in two ranges of the manganese oxidation state, *viz*., $+2.94 \leqslant V_{Mn} \leqslant +3.26$ (the weakly oxidised range) and $+3.82 \leqslant V_{Mn} \leqslant +4.01$ (the strongly oxidised range). In the weakly oxidised range, the *a* parameter decreases whereas the *b* parameter increases. Conversely, in the strongly oxidised range, the *a* parameter increases whereas the *b* parameter decreases. The unit cell vectors and the space group also undergo changes. In the weakly oxidised range, the brownmillerite structure is retained. In the strongly oxidised range, the intensity of the *hkl* reflections with $k \neq 2n$ becomes zero, which corresponds to a transition to a new unit cell with the following parameters: $a \approx c \approx \sqrt{2}a_{per}$, $b \approx 2a_{per}$ and space group *Bmmm*. A progressive decrease in the degree of the orthorhombic distortion for $Sr_2MnGaO_{5.505}$ ultimately gives rise to a tetragonal unit cell with $a \approx a_{per}$, $c \approx 2a_{per}$ and space group *P*4/*mmm* (Fig. 15). For the oxidised phase $Sr_2MnGaO_{5.5}$, an orthorhombic structure was established[48] based on the neutron diffraction data (see Table 3). It is likely that discrepancies in the crystallographic symmetry suggested for this compound by different authors (see Refs 48, 51, 52, 56) arise due to different procedures used for the preparation of different samples or variable oxygen content in these samples, which lies within the accuracy limits of the available determination methods.

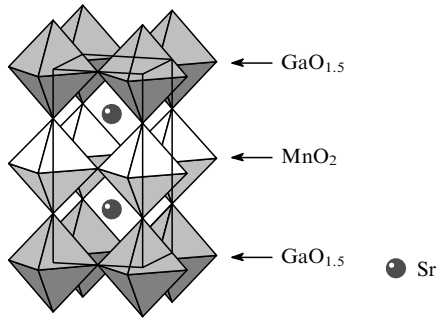


Figure 15. The crystal structure of $Sr_2MnGaO_{5.5}$.

The character of structural changes that occur upon oxidation of $Ca_2MnGaO_{5+\delta}$ and $Sr_2MnGaO_{5+\delta}$ is similar to that induced by insertion of fluorine atoms into the structure of brownmillerite $LaACuGaO_5$ (A = Ca, Sr).[57] In the case of A = Sr, fluorination of $LaACuGaO_5$ yields a tetragonal phase with $a \approx a_{per}$, $c \approx 2a_{per}$, whereas in the case of A = Ca, the orthorhombic symmetry is retained although the degree of the orthorhombic distortion substantially decreases. Similarly, oxidation of Mn-containing brownmillerites gives rise to a tetragonal structure only for A = Sr. According to X-ray diffraction, the structure of the tetragonal phase $Sr_2MnGaO_{5.5}$ is similar to that of oxofluoride $LaSrCuGa(O,F)_{6-\delta}$ (see Refs 53, 57). Probably, the differences in the oxidation of the Ca- and Sr-containing phases are due to steric hindrance associated with insertion of overstoichiometric oxygen atoms. The coordination number of the A cation in the tetragonal structure *P*4/*mmm* should be equal to 12 provided all anion sites are fully occupied or 11 if 1/4 of the oxygen atoms in the Ga layer are absent as in the case of $Sr_2MnGaO_{5.5}$. Realisation of large coordination numbers is difficult in the case of a Ca system (the ionic radius of Ca^{2+} is 1.35 Å) but possible for the larger Sr^{2+} ion (the ionic radius is 1.44 Å). Meanwhile, fluorination of $LaACuGaO_5$ can be represented as anion exchange $O^{2-} \rightarrow 2F^-$, which does not affect the oxidation state of copper. As a result, strong Jahn–Teller distortions of the CuO_6 octahedra are retained in the structure of oxofluorides $LaACuGa(O,F)_{6-\delta}$ and the perovskite subcell undergoes elongation in the direction perpendicular to the CuO_2 layers owing to orbital ordering. Insertion of oxygen into manganites with the brownmillerite structure proceeds oxidatively and results in suppression of the Jahn–Teller deformation.

In the case of $Sr_2MnGaO_{5+\delta}$, oxygen is inserted into every GaO layer, in contrast to the case of $Ca_2MnGaO_{5+\delta}$. According to a refinement of the crystal structure of $Sr_2MnGaO_{5.46}$, the coordination number of gallium atoms increases from 4 to 5 and their coordination polyhedron is a distorted trigonal bipyramid, although oxygen atoms are not completely ordered in the $GaO_{1+\delta}$ layer. Ordering of oxygen atoms and anion vacancies at certain values of δ can be observed by electron diffraction. For $Sr_2MnGaO_{5.41}$, such ordering lowers the symmetry to the monoclinic space group *P*2/*m* ($a = 10.813$ Å, $b = 8.019$ Å, $c = 8.486$ Å, $\beta = 108.57°$). A structural model of this oxide has been developed based on the analogy between the $GaO_{1+\delta}$ layers and anion-deficient $MnO_{1.5}$ layers in the compounds $A_2B_2O_5$ (A = Ca, Sr, La; B = Mn, Cu),[58–61] $Ca_2MnO_{3.5}$[62] and $Sr_2MnO_{3.5}$ (see Ref. 63). The $Mn(Cu)O_{1.5}$ layers consist of vertex-sharing $Mn(Cu)O_5$ tetragonal pyramids (Fig. 16 *a*,*b*). A probable arrangement of the GaO_5 polyhedra, which agrees with the unit cell parameters and space group symmetry of $Sr_2MnGaO_{5.41}$, is shown in Fig. 16 *c*. In order to convert tetragonal pyramids into GaO_5 trigonal bipyramids, both gallium and oxygen atoms have to be slightly shifted (Fig. 16 *d*).

The observed changes in the unit cell parameters of $Sr_2MnGaO_{5+\delta}$ as a function of the oxygen overstoichiometry δ can be rationalised taking into account the following trends:

— the mean radius of manganese cations decreases with an increase in the oxidation state from +3 to +4 [$r(Mn^{3+}) = 0.79$ Å, $r(Mn^{4+}) = 0.68$ Å];

— the Jahn–Teller distortions of the MnO_6 octahedra are suppressed;

— the degree of distortion of the MnO_2 layers is decreased owing to a smaller tilt angle of the MnO_6 octahedra with respect to the *a* axis;

— the mean Ga–O bond length increases with an increase in the coordination number of gallium atoms due to the appearance of additional oxygen atoms in the Ga layer.

A decrease in the degree of the orthorhombic distortion with an increase in δ occurs as a result of interactions between gallium and inserted oxygen atoms. When the latter occupy vacant anion sites within the $GaO_{1+\delta}$ layer, the distance between two nearest gallium atoms and the additional oxygen atom from neighbouring

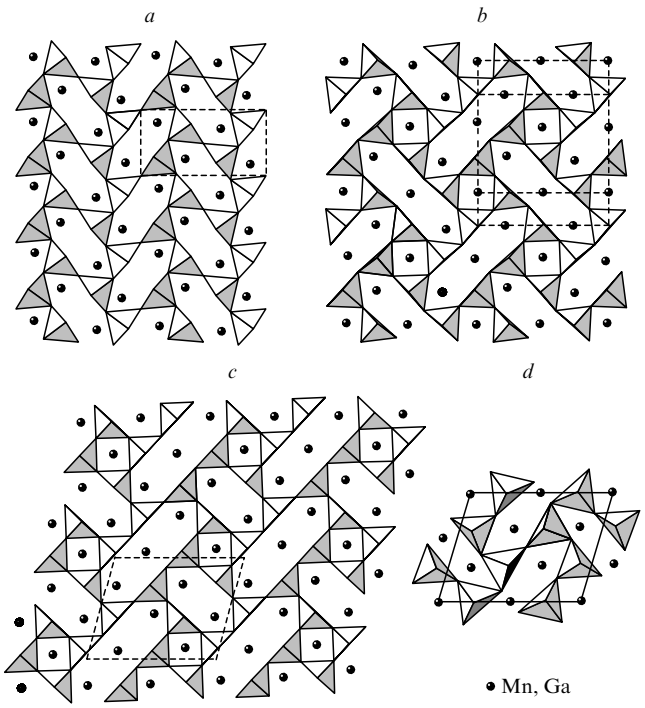


Figure 16. Arrangement of layers composed of the MnO_5 tetragonal pyramids in the structures of $Ca_2Mn_2O_5$, $Ca_2MnO_{3.5}$ (*a*) and $Sr_2MnO_{3.5}$ (*b*) and of the GaO_5 tetragonal pyramids in the structures of $Sr_2MnGaO_{5.41}$ (*c*) (*d* shows the conversion of a GaO_5 tetragonal pyramid into a trigonal bipyramid).

chains of tetrahedra becomes too large. In order to decrease this distance, the gallium atoms from the neighbouring chains shift towards the positions of the B cations in the original perovskite structure thus giving rise to a decrease in the distance between the chains of tetrahedra and the unit cell parameter *c*, the latter being almost linearly dependent on V_{Mn} and, consequently, on δ. The two opposite trends contribute to the change in the parameter *a*. With an increase in the manganese oxidation state in $Sr_2MnGaO_{5+\delta}$, the equatorial Mn – O bond length decreases.

δ	−0.003	0.025	0.13	0.46	0.47
$d(Mn-O)_{eq}$ /Å	1.945(20)	1.9243(5)	1.9222(4)	1.9010(1)	1.8998(1)

In the weakly oxidised range, this leads to a decrease in the *a* parameter and is accompanied by an increase in the degree of distortion of the chains of tetrahedra owing to cooperative rotation of the GaO_4 tetrahedra around the *b* axis by a larger angle, which is reflected in the change in the Ga – O – Ga bond angle from 134.4(5)° in $Sr_2MnGaO_{4.97}$ to 131.4(5)° in $Sr_2MnGaO_{5.025}$. However, further decrease in the degree of the orthorhombic distortion and formation of the tetragonal structure in the strongly oxidised range requires an increase in the Ga – O – Ga angle [*e.g.*, this angle is 165.8(4)° in $Sr_2MnGaO_{5.46}$], which finally leads to an increase in the *a* parameter in this range.

With an increase in the manganese oxidation state, axial distortions of the MnO_6 octahedra progressively decrease affecting the axial Mn – O bond lengths

δ	−0.03	0.025	0.13	0.46	0.5
$d(Mn-O)_{ax}$ /Å	2.411(4)	2.372(5)	2.225(8)	1.983(6)	1.956(3)

Since the axial Mn – O bonds are oriented along the *b* axis, a decrease in the respective unit cell parameter might be expected. Notwithstanding, the *b* parameter increases in the weakly oxidised range. The reason for this is a decrease in the degree of distortions of the MnO_2 layers due to a smaller tilt angle of the MnO_6 octahedra around the *a* axis. The Mn – O – Mn bond angle in the MnO_2 plane increases from 169.5(10)° (δ = −0.03) to 173.7(3)° (δ = 0.025), 176.8(5)° (δ = 0.13) and becomes equal to 180° for δ = 0.46, 0.47, 0.505. Simultaneously, the axial Ga – O bond elongates: 1.816(5) Å (δ = −0.03), 1.847(5) Å (δ = 0.025), 1.977(9) Å (δ = 0.13). As a result of this elongation and subsequent orientation of the axial Mn – O bond lengths parallel to the *b* axis, the *b* parameter in the weakly oxidised range increases despite shortening of the axial Mn – O bond.

VI. Complex oxofluorides $Sr_2MnGaO_{5-x}F_{1+x}$

In addition to oxygen atoms, fluorine atoms can also be used to modify the composition of the anion sublattice and the manganese oxidation state in brownmillerite Sr_2MnGaO_5. Oxygen and fluorine atoms are similar in terms of their crystal chemical properties. Their anions have similar ionic radii (r_{F^-} = 1.29 Å, $r_{O^{2-}}$ = 1.35 Å for the coordination number of 2). Several examples of successful insertion of fluorine into the structures of complex manganese oxides resulting in respective oxofluorides have been reported, including $Sr_2Mn_2O_{5-x}F_{1+x}$,[64] $LaSrMnO_4F$ (Ref. 65) and $La_{1.2}Sr_{1.8}Mn_2O_7F_2$.[66] As has been shown recently,[57] fluorine-derivatives of copper-contaning brownmillerites $LaACuGaO_5$ (A = Ca, Sr) can be synthesised using XeF_2 as a fluorinating agent. A similar method was applied to the synthesis of oxofluorides $Sr_2MnGaO_{5-x}F_{1+x}$. A detailed discussion of the utilisation of xenon difluoride for the fluorination of complex oxides and analysis of the processes accompanying fluorination may be found in a recent review.[67] Oxofluorides $Sr_2MnGaO_{5-x}F_{1+x}$ were synthesised starting from completely oxidised $Sr_2MnGaO_{5.5}$ at 500 – 600 °C using an anion exchange reaction, which gives rise to a decrease in the formal oxidation state of manganese.[56, 68]

$$Sr_2MnGaO_{5.5} + \frac{1+x}{2}XeF_2 \longrightarrow$$

$$\longrightarrow Sr_2MnGaO_{5-x}F_{1+x} + \left(\frac{1}{2}+x\right)[O] + \frac{1+x}{2}Xe.$$

Chemical reduction in the reaction with xenon difluoride is achieved owing to involvement of the walls of the copper tube that is used as the reactor. Oxygen evolved upon anion exchange is adsorbed by the walls giving rise to the Cu/Cu_2O getter, which regulates the partial oxygen pressure in the course of the reaction. Oxofluorides $Sr_2MnGaO_{5-x}F_{1+x}$ crystallise in the tetragonal system (sp. gr. *P*4/*mmm*) with the following unit cell parameters: $a \approx a_{per}$, $c \approx 2a_{per}$ (Table 5). According to a calculation of the bond valence sum and crystal lattice energy, partial substitution of fluorine for oxygen and insertion of excess fluorine atoms takes place in the Ga layers. Consequently, all vacancies in these layers become filled giving rise to the stoichiometry $GaO_{1-x}F_{1+x}$. It is of interest to analyse changes in the behaviour of the compound Sr_2MnGaO_5 doped with either fluorine or oxygen as a function of the manganese oxidation state. The changes in the Mn – O bond lengths for the fluorinated and oxidised phases are plotted in Fig. 17 *a*. In both cases, the equatorial Mn – O bonds in the MnO_6 octahedra elongate with a decrease in V_{Mn} (which is equivalent to a decrease in δ or an increase in the fluorine content) from 1.8998 Å (V_{Mn} = +4) to 1.9222 Å (V_{Mn} = +3.26, δ = 0.13)[51]

Table 5. The crystallographic data for oxofluorides $Sr_2MnGaO_{5-x}F_{1+x}$.

Fluorination conditions	Unit cell parameters /Å		V_{Mn}
	a	*c*	
Starting oxide (without XeF_2)	3.8003(7)	7.948(3)	+4.00
1 : 1 XeF_2, 500 °C, 10 h	3.8557(3)	7.7843(8)	+3.78
1 : 1 XeF_2, 600 °C, 20 h	3.865(1)	7.779(3)	+3.54
1 : 3 XeF_2, 600 °C, 20 h	3.8794(3)	7.7328(6)	+3.39

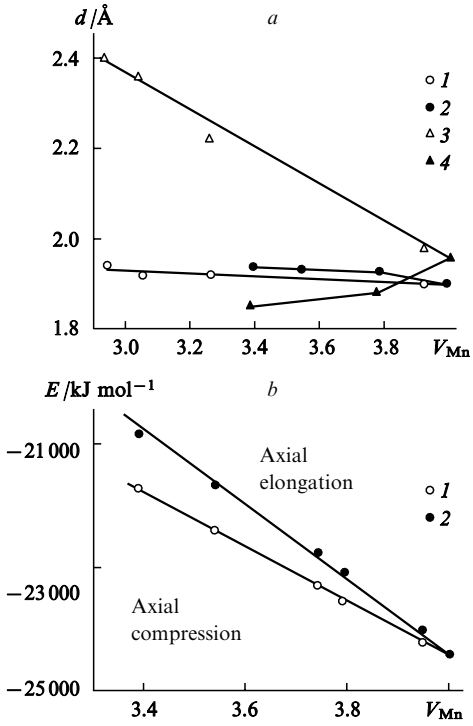


Figure 17. Changes in the $(Mn-O)_{eq}$ (*1*, *2*) and $(Mn-O)_{ax}$ (*3*, *4*) bond lengths in $Sr_2MnGaO_{5+\delta}$ (*1*, *3*) and $Sr_2MnGaO_{5-x}F_{1+x}$ (*2*, *4*) (*a*) and in the crystal lattice energy for $Sr_2MnGaO_{5-x}F_{1+x}$ in the case of axially compressed (*1*) and axially elongated (*2*) MnO_6 octahedra (*b*) as a function of the manganese oxidation state.

and further to 1.9411 Å ($V_{Mn} = +3.39$, $x_F = 0.61$) owing to an increase in the ionic radius of manganese upon reduction.

In the case of $Sr_2MnGaO_{5+\delta}$ ($\delta \approx 0.5$), reduction is also accompanied by an elongation of the axial Mn–O bonds due to the Jahn–Teller effect. Conversely, a progressive compression of the MnO_6 octahedra with a decrease in the manganese oxidation state is observed for solid solutions $Sr_2MnGaO_{5-x}F_{1+x}$. The axial Mn–O bonds in $Sr_2MnGaO_{4.78}F_{1.22}$ [*viz.*, 1.876(8) Å] are significantly shorter than in $Sr_2MnGaO_{5.5}$ [1.956(3) Å]. Thus, the reductive fluorination leads to a change in the type of Jahn–Teller effect from axially elongated to axially compressed. Presumably, this is due to competitive changes in the lattice energy and stabilisation energy associated with the Jahn–Teller distortion of the octahedral environment of manganese atoms.

In manganites $Sr_2MnGaO_{5+\delta}$ doped with oxygen, the axial elongation of the MnO_6 octahedra is partly compensated by shortening of the axial Ga–O bonds due to a decrease in the coordination number of gallium to 4. For solid solutions $Sr_2MnGaO_{5-x}F_{1+x}$, the axial Ga–O bond lengths remain constant upon variation of the composition of the solid solution since all anion sites in the Ga layer are already occupied and thus the coordination number of gallium atoms does not change. Therefore, in this case, the elongation of the axial Ga–O bond coupled with the lack of a compensating contraction should result in too long Sr–O bonds and thus in inevitable losses in the crystal lattice energy (Fig. 17 *b*).

The change in the type of Jahn–Teller distortion on going from $Sr_2MnGaO_{5.5}$ to $Sr_2MnGaO_{5-x}F_{1+x}$ should give rise to a change in the type of orbital ordering, as it was established for solid solutions $Nd_{1-x}Sr_xMnO_3$.[69] A change in the strontium/neodymium stoichiometric ratio and, consequently, in the manganese oxidation state results, at $x = 0.6$, in a change in the type of Jahn–Teller distortion from axially compressed [$0.55 < x < 0.6$, $d(Mn-O)_{eq} = 1.948$ Å, $d(Mn-O)_{ax} = 1.906$ Å] to axially elongated [$x > 0.6$, $d(Mn-O)_{eq} = 1.894$ Å, $d(Mn-O)_{ax} = 1.955$ Å]. The reason for the change in the type of Jahn–Teller distortion is the change of the type of orbital ordering from $d(x^2-y^2)$ to $d(z^2)$, which, in turn, is accompanied by a change in the magnetic structure from type A (antiferromagnetically ordered ferromagnetic planes) to type C (ferromagnetically ordered antiferromagnetic planes) and a metal–dielectric transition at $x = 0.6$.

VII. Magnetic and transport properties of brownmillerites $A_2MnB'O_{5+\delta}$ (A = Ca, Sr; B′ = Ga, Al) and their derivatives

Despite differences in the crystal structures of brownmillerites $A_2MnB'O_{5+\delta}$ (A = Ca, Sr; B′ = Ga, Al) with $\delta \approx 0$ due to different ordering patterns of the chains of tetrahedra, their magnetic structures are essentially similar. These phases convert into an antiferromagnetic state at $T_N = 150-180$ K. The respective saturated magnetic moments (μ) and the Néel temperatures (T_N), as determined by neutron diffraction for several compositions, are listed in Table 6. The magnitudes of the magnetic moments are in good agreement with the theoretical values for Mn^{3+} (which is characterised by the electronic configuration $3d^4$, $t_{2g}^3e_g^1$). The magnetic moments of manganese atoms are oriented perpendicular to the MnO_2 layers. All reduced brownmillerites reveal the G-type antiferromagnetic structure, which implies that the magnetic unit cell conforms to the crystallographic one and the magnetic moments of adjacent manganese atoms are antiparallel not only in the MnO_2 layers but between the layers as well (Fig. 18 *a*).

The magnetic interaction in the brownmillerite structure has a three-dimensional character despite the fact that the distances between adjacent Mn atoms along the *b* axis are approximately twice as large as in the *ac* plane. The three-dimensional character of the magnetic ordering assumes significant superexchange interactions between consecutive MnO_2 layers along the *b* direc-

Table 6. The magnetic characteristics of brownmillerites $A_2MnB'O_{5+\delta}$ (A = Ca, Sr; B′ = Ga, Al).

Oxide	μ /μ_B	T_N /K	Ref.
Ca_2MnAlO_5	3.53(2)	152	41
Ca_2MnGaO_5	3.61(5)	160	52
$SrCaMnGaO_5$	3.30(2)	180	43
Sr_2MnGaO_5	3.16(6)	183	52
	3.26(3)	180	41
$Sr_2MnGaO_{5.5}$	2.1(1)	110	52

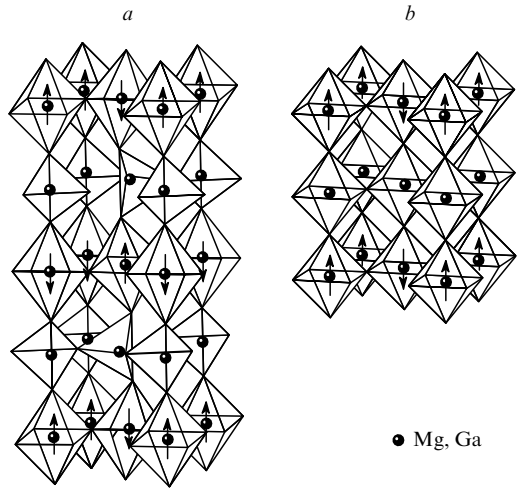


Figure 18. The magnetic structure of Sr_2MnGaO_5 (G-type) (*a*) and $Sr_2MnGaO_{5.5}$ (C-type) (*b*).

tion of the orthorhombic unit cell. The involvement of the superexchange interactions is directly supported by the NQR data.[55] The frequency of the local magnetic field on a gallium atom exceeds the calculated frequency of a dipole field by two orders of magnitude. This suggests that the experimentally observed local field has a dominant contact character and is induced by the superexchange interactions between manganese ions through a 'nonmagnetic' GaO_4 tetrahedron. The magnetic structure of $Sr_2MnGaO_{5.5}$, although also antiferromagnetic, is different from that of the reduced compound. In this structure, the MnO_2 layers (in which manganese atoms are ordered antiferromagnetically) are coupled ferromagnetically, which corresponds to type C of the perovskite magnetic structures (Fig. 18 *b*). The magnetic unit cell remains tetragonal although its volume is twice as large as that of the crystallographic cell. The parameters of the magnetic and crystallographic unit cells relate to each other by the following equations: $a_m = \sqrt{2}a_c$, $c_m = c_c$. The changes in the magnetic structure type on going from Sr_2MnGaO_5 to $Sr_2MnGaO_{5.5}$ occur due to the appearance of extra oxygen atoms in the Ga layers, which additionally stabilise the type C magnetic structure due to more distant 'diagonal' superexchange interactions through the GaO_6 octahedra.[52] Interactions through the $Ga(O,F)_6$ octahedra in $Sr_2MnGaO_{5-x}F_{1+x}$ [$T_N = 70$ K, $\mu = 1.5(1)\ \mu_B$] also give rise to ferromagnetic ordering of antiferromagnetic planes.[70] Nevertheless, in contrast to Sr_2MnGaO_5 and $Sr_2MnGaO_{5.5}$, the orientation of the magnetic moments in oxofluorides is parallel to the MnO_2 layers rather than perpendicular to them, which can be explained assuming the change in the orbital ordering type. This was suggested based on the analysis of interatomic distances in the structures of oxofluorides.[68]

According to neutron diffraction and muon resonance spectroscopy, $Sr_2MnGaO_{5.5}$ is characterised by an inhomogeneous magnetic structure below 180 K. This manifests itself in the appearance of small domains ($\sim$40 Å) with the type G magnetic structure embedded into a matrix with the type C structure.[52] When the oxygen overstoichiometry index δ is decreased to 0.41, the local magnetic order of the type G is replaced by co-existence of two regular magnetic structures: an antiferromagnetic type G structure is formed at $T = 140$ K while an admixture of a type C phase appears at $T = 110$ K.[71] The co-existence of these two long-range magnetic structures was observed for $Sr_2MnGaO_{5.5}$ as well (see Ref. 48). It is the local ordering of oxygen atoms in the $GaO_{1+\delta}$ layer giving rise to differences in the character of interactions between adjacent MnO_2 layers that should be considered as the most probable reason for this phenomenon. Indeed, such an ordering, which results in the symmetry lowering to monoclinic system, was experimentally established for $Sr_2MnGaO_{5.41}$ (see Refs 51, 56).

Complex oxides $Ca_2MnGaO_{5.045}$, $Ca_2MnGa_{1-x}Zn_xO_5$ ($x = 0.1-0.2$)[55] and $SrCaMnGaO_5$ (see Ref. 43) are insulators. Their electrical resistance as a function of temperature follows the normal activation law with sufficient accuracy. $SrCaMnGaO_5$ manifests magnetoresistance that amounts to 85% in a field of 6 T and up to 90% in a field of 13 T at 159 K.[43]

VIII. The oxide $Ca_{2.5}Sr_{0.5}GaMn_2O_8$ as the second member of the homologous series of brownmillerite-like structures

The homologous series of brownmillerite structures $A_{n+1}B_nB'O_{3n+2}$ is formally constructed by adding a certain number of octahedral layers to the brownmillerite structure. The *n*th member of the series contains blocks composed of *n* layers of BO_6 octahedra separated from each other by a layer of $B'O_4$ tetrahedra. The second member of the manganese-containing homologous series, which corresponds to stoichiometry $Ca_{2.5}Sr_{0.5}GaMn_2O_8$, was synthesised at 1100 °C in air.[72] Since the formal oxidation state of manganese in this compound is +3.5, the synthesis does not require an inert atmosphere. This

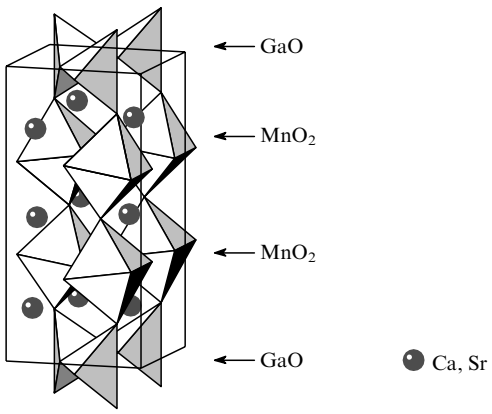


Figure 19. The crystal structure of $Ca_{2.5}Sr_{0.5}GaMn_2O_8$.

oxide crystallises in the orthorhombic system [sp. gr. $Pcm2_1$, $a = 5.4294(1)$ Å, $b = 11.3722(3)$ Å, $c = 5.2983(1)$ Å] (Fig. 19). In this structure, the MnO_6 octahedra are distorted but the character of the distortion differs from that in brownmillerite. An MnO_6 octahedron is characterised by five shorter [1.857(10) – 1.950(4) Å] and one longer [2.163(5) Å] Mn – O bonds. The elongated axial Mn – O bond is directed towards the layer of tetrahedra whereas the short axial bond is responsible for the Mn – O – Mn bonding between the layers of octahedra. Apparently, such an atomic arrangement provides the optimum coordination of the A cations located between the octahedral layers. This oxide converts between 150 K and 125 K into an antiferromagnetically ordered state with the magnetic moments oriented perpendicular to the MnO_2 layers [$\mu = 3.09(1)\ \mu_B$]. Within the MnO_2 layer, the neighbouring manganese atoms interact antiferromagnetically whereas adjacent octahedral layers and their pairs separated from each other by a GaO layer interact ferromagnetically. The transition into the magnetically ordered state is accompanied by an abrupt decrease in the electrical resistance (which, notwithstanding, remains too high to refer this transition to a dielectric – metal transition) with the magnetoresistance effect being about 50% in a field of 80 kŒ.[72]

Reduction of manganese in $Ca_{2.5}Sr_{0.5}GaMn_2O_8$ by means of partial substitution of trivalent cations for bivalent cations of alkaline-earth metals gives rise to a structural transformation resulting in a new type of anion ordering, which has been observed for the first time in the crystal structure of $Sr_{0.7}Y_{0.3}CoO_{2.62}$ (see Ref. 73). The oxide $Y_{0.8}Sr_{2.2}GaMn_2O_{7.9}$ is characterised by a tetragonal unit cell with the following parameters: $a = 7.6373(3)$ Å and $c = 15.6636(10)$ Å, sp. gr. $I4/mmm$.[74] This structure is composed of alternating octahedral and tetrahedral layers; the B sites are statistically occupied by manganese and gallium atoms with manganese atoms preferably occupying the octahedral sites. The structure of $Y_{0.8}Sr_{2.2}GaMn_2O_{7.9}$ contains isolated squares of vertex-sharing tetradera instead of chains of tetrahedra typical of the brownmillerite structure. The coordination environment of the B cations within this layer is supplemented by additional oxygen atoms situated between the squares of tetrahedra giving rise to a total coordination number of 5.[74] Presumably, the driving force for the formation of this structure is ordering of crystallographically non-equivalent Sr^{2+} and Y^{3+} cations.

IX. Conclusion

It is the differences in the ionic radii, electronic structures and typical coordination polyhedra of various cations differing in their crystal chemical properties that can be deliberately exploited in the design and synthesis of layered perovskite-like compounds. This idea is demonstrated in the present review by the example of complex oxides $A_2MnB'O_{5+\delta}$ (A = Ca, Sr; B′ = Ga, Al) having

the brownmillerite structure. A method for the synthesis of such complex oxides has to provide the optimum conditions (including a proper choice of composition, temperature and partial oxygen pressure) for ordering of cations. The presence of anion vacancies in the brownmillerite structure enables chemical modifications of the structure and adjustments of properties by variations of the anion stoichiometry under mild conditions not affecting the initially achieved ordered arrangement of cations. The brownmillerite structure is capable of adapting to changes in the anion composition (owing to the anion-deficient B′O layers); it is characterised by stable octahedral environment of manganese atoms in the oxidation states +3 and +4; it allows preparation of various members of the homologous series $A_{n+1}B_nB'O_{3n+2}$ manifesting magnetoresistance (for $n = 1, 2$). Thanks to all these features, browmillerite-like complex oxides of manganese should be considered as highly promising objects for the synthesis of novel magnetoresistive materials.

The current review has been written with partial financial support from the 'Petroleum Research Fund' (Project No. 38459-AC5), the INTAS (Grant for young scientists YSF 03-55-1035) and the 'Federal Programme in Support of the Leading Scientific Schools of the Russian Federation' (Project NSch-2033.2003.03). The authors are grateful to colleagues from the Laboratory for Inorganic Crystal Chemistry at the Department of Chemistry, MSU and Laboratory for Electron Microscopy at Antwerp University (EMAT, RUCA) for help in the research work and fruitful discussions. A M Abakumov also acknowledges financial support from the Charitable fund of the Russian Academy of Sciences.

References

1. R V Helmot, J Wecker, B Holzapfel, L Schultz, K Samwer *Phys. Rev. Lett.* **71** 2331 (1993)
2. S Jin, T H Tiefel, M McCormack, R A Fastnacht, R Ramesh, L H Chen *Science* **264** 413 (1994)
3. C N R Rao, A K Cheetham *Science* **272** 369 (1996)
4. A P Ramirez *J. Phys.: Condens. Matter* **9** 8171 (1997)
5. Y Tokura, Y Tomioka, H Kuwahara, A Asamitsu, Y Morimoto, M Kasai *J. Appl. Phys.* **79** 5288 (1996)
6. J M D Coey, M Viret, S von Molnar *Adv. Phys.* **48** 167 (1999)
7. J B Goodenough *Phys. Rev.* **100** 564 (1955)
8. J B Goodenough *J. Appl. Phys.* **81** 5330 (1997)
9. D I Khomskii, G A Sawatsky *Solid State Commun.* **102** 87 (1997)
10. C N R Rao, A Arulraj, P N Santosh, A K Cheetham *Chem. Mater.* **10** 2714 (1998)
11. Y Morimoto, A Asamitsu, H Kuwahara, Y Tokura *Nature (London)* **380** 141 (1996)
12. T Kimura, Y Tomioka, H Kuwahara, A Asamitsu, M Tamura, Y Tokura *Science* **274** 1698 (1996)
13. P D Battle, S J Blundell, M A Green, W Hayes, M Honold, A K Klehe, N S Laskey, J E Millburn, L Murphy, M J Rosseinsky, N A Samarin, J Singleton, N A Sluchanko, S P Sullivan, J F Vente *J. Phys.: Condens. Matter* **8** L427 (1996)
14. R Seshardi, C Martin, A Maignan, M Hervieu, B Raveau, C N R Rao *J. Mater. Chem.* **6** 1585 (1996)
15. H Asano, J Hayakawa, M Matsui *Phys. Rev. B* **56** 5395 (1997)
16. G Blasse *J. Inorg. Nucl. Chem.* **27** 2863 (1965)
17. A Benabad, A Daoudi, R Salmon, C Le Flem *J. Solid State Chem.* **22** 121 (1977)
18. J M Tarascon, Y Le Page, W R McKinnon, E Tselepis, P Barboux, B G Bagley, R Ramesh *Mater. Res. Soc. Symp. Proc.* **156** 317 (1989)
19. M Catti, G Dalba, P Fornasini, M Molgg *J. Solid State Chem.* **112** 392 (1994)
20. M Herview, C Michel, D Pelloquin, A Maignan, B Raveau *J. Solid State Chem.* **132** 420 (1997)
21. T P Beales, M Molgg, J R Gorton, D C Sinclair *Mater. Res. Bull.* **31** 1543 (1996)
22. J T Vaughey, J B Wiley, K R Poppelmeier *Z. Anorg. Allg. Chem.*, **598**/**599** 321 (1991)
23. G Roth, P Adelmann, R Knitter, S Massing, Th Wolf *J. Solid State Chem.* **99** 376 (1992)
24. A L Kharlanov, I Bryntse, E V Antipov, A V Luzikova *Acta Chem. Scand.* **47** 434 (1993)
25. A V Luzikova, A L Kharlanov, E V Antipov, H Müller-Bushbaum *Z. Anorg. Allg. Chem.* **620** 326 (1994)
26. F Puertas, M T Blanco Varela, R Dominguez *Cem. Concr. Res.* **20** 429 (1990)
27. T Krekels, O Milat, G Van Tendeloo, S Amelinckx, T G N Babu, A J Wright, C Greaves *J. Solid State Chem.* **105** 313 (1993)
28. O Milat, T Krekels, G Van Tendeloo, S Amelinckx *J. Phys. I* **3** 1219 (1993)
29. M L Ruiz-Gonzalez, C Prieto, J Alonso, J Ramirez-Castellanos, J M Gonzalez-Calbet *Chem. Mater.* **14** 2055 (2002)
30. P Berastegui, S Hull, F J Garcia-Garcia, S-G Eriksson *J. Solid State Chem.* **164** 119 (2002)
31. S Lambert, H Leligny, D Grebille, D Pelloquin, B Raveau *Chem. Mater.* **14** 1818 (2002)
32. *International Tables for Crystallography* Vol. 1 (London: Kluwer Academic, 1999) p. 899
33. A A Colville *Acta Crystallogr., Sect. B* **26** 1469 (1970)
34. J Berggren *Acta Chem. Scand.* **25** 3616 (1971)
35. P Berastegui, S-G Eriksson, S Hull *Mater. Res. Bull.* **34** 303 (1999)
36. C Greaves, A J Jacobson, B C Tofield, B E F Fender *Acta Crystallogr., Sect. B* **31** 641 (1975)
37. M Schmidt, S G Campbell *J. Solid State Chem.* **156** 292 (2001)
38. A A Colville, S Geller *Acta Crystallogr., Sect. B* **27** 2311 (1971)
39. R Arpe, R von Schenck, H Müller-Bushbaum *Z. Anorg. Allg. Chem.* **410** 97 (1974)
40. A M Abakumov, M G Rozova, B Ph Pavlyuk, M V Lobanov, E V Antipov, O I Lebedev, G Van Tendeloo, D V Sheptyakov, A M Balagurov, F Bouree *J. Solid State Chem.* **158** 100 (2001)
41. A J Wright, H M Palmer, P A Anderson, C Greaves *J. Mater. Chem.* **12** 978 (2002)
42. A J Wright, H M Palmer, P A Anderson, C Greaves *J. Mater. Chem.* **11** 1324 (2001)
43. P D Battle, A M Bell, S J Blundell, A I Coldea, D J Gallon, F L Pratt, M J Rosseinsky, C A Steer *J. Solid State Chem.* **167** 188 (2002)
44. J Toepfer, J B Goodenough *Eur. J. Solid State Inorg. Chem.* **34** 467 (1997)
45. E J Cussen, M J Rosseinsky, P D Battle, J C Burley, L E Spring, J F Vente, S J Blundell, A I Coldea, J Singleton *J. Am. Chem. Soc.* **123** 1111 (2001)
46. A I Coldea, S J Blundell, I M Marshall, C A Steer, J Singleton, F L Pratt, L D Noailles, M J Rosseinsky, L E Spring, P D Battle *Phys. Rev. B* **65** 054402 (2001)
47. P D Battle, S J Blundell, J B Claridge, A I Coldea, E J Cussen, L D Noailles, M J Rosseinsky, J Singleton, J Sloan *Chem. Mater.* **14** 425 (2002)
48. E N Caspi, M Avdeev, S Short, J D Jorgensen, B Dabrowski, O Chmaissem, J Mais, S Kolesnik *J. Solid State Chem.* **177** 1456 (2004)
49. A M Abakumov, M G Rozova, B Ph Pavlyuk, M V Lobanov, E V Antipov, O I Lebedev, G Van Tendeloo, O L Ignatchik, E A Ovtchenkov, Yu A Koksharov, A N Vasil'ev *J. Solid State Chem.* **160** 353 (2001)
50. A M Abakumov, M G Rozova, A M Alekseeva, M V Lobanov, E V Antipov, O I Lebedev, G Van Tendeloo, D V Sheptyakov, A M Balagurov *Z. Anorg. Allg. Chem.* **628** 2233 (2002)
51. A M Abakumov, M G Rozova, A M Alekseeva, M L Kovba, E V Antipov, O I Lebedev, G Van Tendeloo *Solid State Sci.* **5** 871 (2003)
52. V Yu Pomyakushin, A M Balagurov, T V Elzhov, D V Sheptyakov, P Fisher, D I Khomskii, V Yu Yushankhai, A M Abakumov, M G Rozova, E V Antipov, M V Lobanov, S J L Billinge *Phys. Rev. B* **66** 184412 (2002)
53. D V Sheptyakov, A M Abakumov, E V Antipov, A M Balagurov, S J L Billinge, P Fisher, L Keller, M V Lobanov, B Ph Pavlyuk, V Yu Pomyakushin, M G Rozova *Appl. Phys. A* **74** S1734 (2002)

54. A M Abakumov, A M Alekseeva, M G Rozova, E V Antipov, O I Lebedev, G Van Tendeloo *J. Solid State Chem.* **174** 319 (2003)
55. M V Lobanov, Candidate Thesis in Chemical Sciences, Moscow State University, Moscow, 2000
56. E V Antipov, A M Abakumov, A M Alekseeva, M G Rozova, J Hadermann, O I Lebedev, G Van Tendeloo *Phys. Status Solidi A* 1 (2004)
57. J Hadermann, G Van Tendeloo, A M Abakumov, B Ph Pavlyuk, M Rozova, E V Antipov *Int. J. Inorg. Mater.* **2** 493 (2000)
58. K R Poeppelmeier, M E Leonowicz, J M Longo *J. Solid State Chem.* **44** 89 (1982)
59. K R Poeppelmeier, M E Leonowicz, J C Scanlon, J M Longo, W B Yelon *J. Solid State Chem.* **45** 71(1982)
60. V Caignaert, N Nguyen, M Hervieu, B Raveau *Mater. Res. Bull.* **20** 479 (1985)
61. N R Khasanova, F Izumi, Z Hiroi, M Takano, Q Huang, A Santoro *Acta Crystallogr., Sect. C* **52** 2381 (1996)
62. M E Leonowicz, K R Poeppelmeier, J M Longo *J. Solid State Chem.* **58** 71 (1985)
63. L J Gillie, A J Wright, J Hadermann, G Van Tendeloo, C Greaves *J. Solid State Chem.* **167** 145 (2002)
64. M V Lobanov, A M Abakumov, A V Sidorova, M G Rozova, O G D'yachenko, E V Antipov, J Hadermann, G Van Tendeloo *Solid State Sci.* **4** 19 (2002)
65. L D Aikens, R K Li, C Greaves *Chem. Commun.* **21** 2129 (2000)
66. C Greaves, J L Kissick, M G Francesconi, L D Aikens, L J Gillie *J. Mater. Chem.* **9** 111 (1999)
67. A M Abakumov, M G Rozova, E I Ardashnikova, E V Antipov *Usp. Khim.* **71** 443 (2002) [*Russ. Chem. Rev.* **71** 383 (2002)]
68. A M Alekseeva, A M Abakumov, M G Rozova, E V Antipov, J Hadermann *J. Solid State Chem.* **177** 731 (2004)
69. R Kajimoto, H Yoshizawa, H Kawano, H Kuwahara, Y Tokura, K Ohoyama, M Ohashi *Phys. Rev. B* **60** 9506 (1999)
70. V Pomjakushin, D Sheptyakov, P Fischer, A Balagurov, A Abakumov, M Alekseeva, M Rozova, E Antipov, D Khomskii, V Yushankhai *J. Magn. Magn. Mater.* (2004) (in the press)
71. V Pomjakushin, D Sheptyakov, P Fischer, A Balagurov, A Abakumov, M Alekseeva, M Rozova, E Antipov *Phys. Rev. B* (2004) (in the press)
72. P D Battle, S J Blundell, P N Santhosh, M J Rosseinsky, C Steer *J. Phys.: Condens. Matter* **14** 13 569 (2002)
73. S Ya Istomin, J Grins, G Svensson, O A Drozhzhin, V L Kozhevnikov, E V Antipov, J P Attfield *Chem. Mater.* **15** 4012 (2003)
74. L J Gillie, H M Palmer, A J Wright, J Hadermann, G Van Tendeloo, C Greaves *J. Phys. Chem. Solids* **65** 87 (2004)